Received May 2000
Revised December 2000
Accepted December 2000

Computation of flow and heat transfer in two-dimensional rib-roughened passages, using low-Reynolds-number turbulence models

H. Iacovides and M. Raisee
Department of Mechanical Engineering, UMIST, Manchester, UK

Keywords *Thermal convection, Heat transfer, Turbulence, Modelling, Channels, Pipes*

Abstract *Low-Re turbulence models are used in the computation of convective heat transfer in two-dimensional ribbed passages. The cases computed include ribbed annular channels, pipes and plane channels. The models investigated cover both zonal models, that obtain the near-wall dissipation rate from the wall distance, and full low-Re models. Effective viscosity modes and simple (basic) second-moment closures are used. Zonal models display predictive weaknesses in the rib-induced separation region, but return reasonable heat transfer levels. For the low-Re models an alternative length-scale-correction term to the one proposed by Yap is developed, which is independent of the wall distance. This wall-independent correction term is found to improve heat transfer predictions, especially for the low-Re k-ε model. The low-Re models produce a more realistic heat transfer variation in the separation region and reasonable Nusselt number levels. The differential second-moment closure (DSM) models improve heat transfer predictions after re-attachment and over the rib surface. The effect of Reynolds number on the Nusselt number is not, however, fully reproduced by the models tested.*

1. Introduction

Heat-transfer-enhancing ribs are employed in blade and also in other cooling applications. For blade cooling, such ribs are used along the surfaces of internal passages within rotating blades. As intended, ribs cause flow separation and a rise in turbulence and heat transfer levels. It is consequently important that turbulence models employed in the computation of blade-cooling flows are able to account for the effects of rib-roughness on turbulence.

The flow and thermal developments in blade-cooling passages are also strongly influenced by the presence of U-bends of strong curvature and also by the blade rotation. The computation of flow and heat transfer through curved and rotating passages has been the focus of numerous investigations, both within the authors' group (Iacovides and Launder, 1995) and elsewhere (Besserman and Tanrikut, 1991). As shown in earlier studies, the prediction of the secondary motion generated by curvature requires the resolution of the mean flow across the wall sub-layer, making the wall function approach

International Journal of Numerical Methods for Heat & Fluid Flow, Vol. 11 No. 2, 2001, pp. 138-155.

The authors wish to express their gratitude to Professor B.E. Launder for his support and encouragement. Support for this work has been provided by Rolls-Royce plc and DRA Pyestock. The helpful input of Mr J. Coupland, of Rolls-Royce plc is gratefully acknowledged.

inappropriate. In U-ducts of curvature strong enough to cause flow separation and also in rotating ducts, use of low-Re second-moment closures further improves predictions.

Most of the numerical studies of flow and heat transfer through ribbed passages, such as Lee *et al.* (1988) and Liou *et al.* (1993), have so far employed high-Re models of turbulence with the wall function approach. One exception is the work of Taylor *et al.* (1991) on three-dimensional flows, but comparisons with measurements were not very detailed. Since the other flow features present in blade cooling passages, due to curvature and rotation, necessitate the use of low-Re models of near-wall turbulence, more extensive testing of low-Re models in ribbed passages is necessary, to establish which low-Re models can reliably reproduce the effects of ribs as well as those of orthogonal rotation and strong curvature. Hence in this study low-Re turbulence models are used in the computation of flow and heat transfer through two-dimensional ribbed passages. The main objective is to establish how reliably low-Re models, already tested in computations of flow and heat transfer through curved and rotating ducts, can reproduce the effects of rib roughness. The investigation has included both full low-Re transport models and also zonal models, where simpler near-wall models that obtain the dissipation rate from the wall distance are matched to high-Re transport models in the fully turbulent region. In addition to effective viscosity, second-moment closures are also employed.

2. Mean flow equations

All equations included in this and the subsequent section are presented in the compact Cartesian tensor notation, for brevity. In this study, the two-dimensional plane and axi-symmetric forms of these equations have been solved. Moreover, because the data with which the present computations are being compared have been obtained from experiments in which the variations in fluid temperature were small, fluid properties are assumed to remain constant:

- Continuity:

$$\frac{\partial}{\partial x_i}(\rho U_i) = 0. \tag{1}$$

- Momentum transport:

$$\frac{\partial}{\partial x_j}(\rho U_i U_j) = -\frac{\partial P}{\partial x_i}\left[\mu\left(\frac{\partial U_i}{\partial x_j} + \frac{\partial U_j}{\partial x_i}\right) - \rho\overline{u_i u_j}\right]. \tag{2}$$

- Enthalpy transport equation:

$$\frac{\partial}{\partial_{xj}}(\rho U_i T) = \frac{\partial}{\partial x_j}\left(\frac{\mu}{Pr}\frac{\partial T}{\partial x_j} - \rho\overline{u_i t}\right). \tag{3}$$

The terms $\overline{u_i u_j}$ and $\overline{u_j t}$ are known as the turbulent, or Reynolds, stresses and turbulent heat fluxes respectively. They represent the effects of turbulent mixing on the transport of momentum and thermal energy. In order to solve the above system of the mean flow equations, additional equations need to be introduced to provide the distribution of the turbulent stresses and heat fluxes. While exact equations for these variables can be derived, these are impossible to solve because they include further unknown variables. Approximate equations for $\overline{u_i u_j}$ and $\overline{u_j t}$ are introduced instead, known as turbulence modelling equations. These are presented in the next section.

3. Turbulent flow equations

3.1 Effective viscosity models

In both EVM versions employed here, the Reynolds stresses and the turbulent heat fluxes are obtained from the effective viscosity and effective diffusivity approximations, respectively, shown in equations (4) and (5) below:

$$\rho \overline{u_i u_j} = \frac{2}{3} k \delta_{ij} = \mu_t \left(\frac{\partial U_i}{\partial x_j} + \frac{\partial U_j}{\partial x_i} \right) \tag{4}$$

$$\overline{u_i t} = -\frac{\mu_t}{\sigma_T} \frac{\partial T}{\partial x_i}. \tag{5}$$

This is a widely used approach, popular for its numerical robustness, but which produces isotropic turbulence fields, with the turbulence energy distributed equally in all directions ($\overline{u_1^2} = \overline{u_2^2} = \overline{u_3^2} = \frac{2}{3} k$). Turbulence is however anisotropic and in many flows, such as flows with streamline curvature, the mean flow development is sensitive to the anisotropy of turbulence.

Zonal k-e/one-equation model. As the above name suggests, in the fully-turbulent region the standard high-Re version of the k-ε model is used, while in the near-wall regions a low-Re version of a one-equation model of k-transport is employed. This approach allows the resolution of the mean flow across the viscous wall sub-layer, without the need to use an excessively fine near-wall grid.

In the high-Re k-ε the turbulent viscosity that appears in equations (4) and (5) is obtained from the turbulent kinetic energy, k, and its dissipation rate, ε, according to equation (6):

$$\mu_t = \rho c_\mu k^2 / \varepsilon. \tag{6}$$

Two additional transport equations are used to determine the distributions of k and ε, equations (7) and (9) respectively:

$$\frac{\partial}{\partial x_j} (\rho U_j k) = \frac{\partial}{\partial x_j} \left[\left(\mu + \frac{\mu_t}{\sigma_k} \right) \frac{\partial k}{\partial x_j} \right] + P_k - \rho \varepsilon, \tag{7}$$

where

$$P_k = -\rho\,\overline{u_i u_j}\left(\frac{\partial U_i}{\partial x_j}\right) \tag{8}$$

$$\frac{\partial}{\partial x_j}(\rho U_j \varepsilon) = \frac{\partial}{\partial x_j}\left[\left(\mu + \frac{\mu_t}{\sigma_\varepsilon}\right)\frac{\partial \varepsilon}{\partial x_j}\right] + c_{\varepsilon 1}\frac{\varepsilon}{k}P_k - \rho\, c_{\varepsilon 2}\frac{\varepsilon^2}{k}. \tag{9}$$

The term P_k in the k-transport equation (7) represents the generation rate of turbulence and it is obtained through the exact expression given by equation (8).

The terms $\frac{\partial}{\partial x_j}\left(\frac{\mu_t}{\sigma_k}\frac{\partial k}{\partial x_j}\right)$ approximate the transport of k and ε respectively through turbulent mixing, while the last two terms of the ε transport equation (9) approximate the generation and destruction rates of the dissipation rate.

In the near-wall regions equation (7) is still used to obtain the distribution of k, but the dissipation rate, ε, and the turbulent viscosity, μ_t, are obtained from algebraic expressions (10) and (11), proposed by Woolfshtein (1969), that rely on prescribed length scales ℓ_ε and ℓ_μ:

$$\varepsilon = \frac{k^{3/2}}{\ell_\varepsilon} \tag{10}$$

and

$$\mu_t = \rho\, c_\mu \ell_\mu \sqrt{k}. \tag{11}$$

The length scales ℓ_ε and ℓ_μ are obtained from the near-wall distance Y, according to:

$$\ell_\varepsilon = 2.55\ \mathrm{Y}[1 - \exp(-0.263\ \mathrm{y}^*)] \tag{12}$$

$$\ell_\mu = 2.55\ \mathrm{Y}[1 - \exp(-0.016\ \mathrm{y}^*)], \tag{13}$$

where $\mathrm{y}^* \equiv \mathrm{Yk}^{1/2}/\nu$ is the dimensionless wall distance and is used to introduce the damping effect of the wall on turbulence.

Low-Re k-ε model (Launder and Sharma, 1974). This is an extension of the high-Re k-ε that can reproduce the wall damping of turbulence and hence can be used across the viscous sub-layer. The expression for the turbulent viscosity, (14), now includes the damping function f_μ, given by equation (15), in which the damping parameter, $\mathrm{R_t}$, is the local Reynolds number of turbulence, defined as $\mathrm{R_t} \equiv \mathrm{k})^2/(\nu\varepsilon)$:

$$\mu_\mathrm{t} = \rho\, \mathrm{c}_\mu \mathrm{f}_\mu\, \mathrm{k}^2/\varepsilon \tag{14}$$

$$\mathrm{f}_\mu = \exp[-3.4/(1 + 0.02\,\mathrm{R_t})^2]. \tag{15}$$

The last term in the k-transport equation, (16), the only difference between the high- and low-Re versions of this equation, ensures that at the wall the dissipation of turbulence remains finite. The main difference between the high-Re and low Re versions of the e equation, equations (9) and (17) respectively, is the last term in equation (17) which represents the direct effects of viscosity on the larger, energy-containing turbulent eddies:

$$\frac{\partial}{\partial x_j}(\rho U_j k) = \frac{\partial}{\partial x_j}\left[\left(\mu + \frac{\mu_t}{\sigma_k}\right)\frac{\partial k}{\partial x_j}\right] + P_k - \rho\varepsilon = 2\rho\nu\left(\frac{\partial\sqrt{k}}{\partial x_j}\right)^2 \tag{16}$$

$$\frac{\partial}{\partial x_j}(\rho U_j \varepsilon) = \frac{\partial}{\partial x_j}\left[\left(\mu + \frac{\mu_t}{\sigma_\varepsilon}\right)\frac{\partial \varepsilon}{\partial x_j}\right] + c_{\varepsilon 1}\frac{\varepsilon}{k}P_k - \rho\, c_{\varepsilon 2} f_2 \frac{\varepsilon^2}{k} + 2\rho\nu\nu_t\left[\frac{\partial^2 U_i}{\partial x_j \partial x_q}\right]^2. \tag{17}$$

The damping function f_2 for the generation rate of ε is determined with respect to decaying, grid-generated turbulence:

$$f_2 = 1 - 0.3\exp(-R_t^2). \tag{18}$$

3.2 Low-Re DSM models

DSM closures are introduced so that the effects of the anisotropy of turbulence can be taken into account. The DSM closures employed here are rather simple and empirically devised low-Re extensions of the more widely used basic DSM model, which relies on the linear redistribution terms and uses the wall reflection terms. They have evolved from the low-Re ASM closures proposed by Iacovides and Launder (1992) and subsequently extended by Iacovides and Toumpanakis (1993) to low-Re DSM closures. These models were initially applied to the computation of turbulent flows through rotating cavities and recently, by Nikas (2000), to the computation of flow and heat transfer through stationary and rotating U-bends. The low-Re terms, constants and damping functions have been determined with reference to fully-developed pipe flow and have not been changed in any of the subsequent applications.

Instead of the effective viscosity approximation, equation (4), the turbulent stresses are now obtained through the solution of separate transport equations, represented by equation (19):

$$\begin{aligned}\frac{\partial}{\partial x_k}(\rho U_k \overline{u_i u_j}) &= \frac{\partial}{\partial x_k}\left[\left(\mu + \frac{\mu_t}{\sigma_k}\right)\frac{\partial \overline{u_i u_j}}{\partial x_k}\right] \\ &+ P_{ij} - \rho\varepsilon_{ij} + \varphi_{ij} - \left[H_{ij} - \frac{1}{3}H_{kk}\delta_{ij}\right] + J_{ij}.\end{aligned} \tag{19}$$

As in the k and ε transport equations, the transport of the turbulent stresses due to turbulent mixing is modelled through the effective diffusivity concept.

The term P_{ij} denotes the generation rate of the turbulent stresses and is obtained through the exact expression given in equation (20). The term ε_{ij} denotes the dissipation rate of the turbulent stresses which, as shown in equation (21), is assumed to be isotropic when the flow is fully turbulent and proportional to the ratio $\overline{u_i u_j}/k$ at the wall. The function f_ε is zero when the flow is fully turbulent and one at the wall.

$$P_{ij} = -\left(\rho\overline{u_i u_k}\frac{\partial U_j}{\partial x_k} + \rho\,\overline{u_j u_k}\frac{\partial U_i}{\partial x_k}\right) \tag{20}$$

$$\varepsilon_{ij} = \frac{2}{3}(1 - f_\varepsilon)\varepsilon\delta_{ij} + f_\varepsilon\frac{\overline{u_i u_k}}{k}\varepsilon. \tag{21}$$

The term φ_{ij}, given in equation (22), represents the redistribution of turbulent energy among the different components of the Reynolds stress tensor due to fluctuations in the pressure and strain fields. The first two terms denote a linear return to isotropy and isotropisation of production respectively. They are also present in the widely used high-Re version of the DSM closure. Terms φ^{w}_{ij1} and φ^{w}_{ij2}, given in equations (23)-(25), are the conventional wall reflection terms, proposed by Gibson and Launder (1978), to model the "wall-echo" part of the pressure strain correlation, which, near solid surfaces, removes kinetic energy from the fluctuating component normal to the wall and redistributes in the other two directions. They have been devised for the fully turbulent region of a flow over a plane wall and make use of the wall distance x_n and the unit vector normal to the wall n.

$$\varphi_{ij} = -c_1\rho\frac{\varepsilon}{k}\left(\overline{u_i u_j} - \frac{2}{3}k\delta_{ij}\right) - c_2\left(P_{ij} = \frac{1}{2}P_k\delta_{ij}\right) + f_w(\varphi^w_{ij1} + \varphi^w_{ij2}) \tag{22}$$

$$\varphi^w_{ij,1} = c^w_1\rho\frac{\varepsilon}{k}\left(\overline{u_k u_m}n_k n_m\delta_{ij} - \frac{3}{2}\overline{u_k u_i}n_k n_j - \frac{3}{2}\overline{u_k u_j}n_k n_i\right)\left\{\frac{k^{1.5}}{\varepsilon c_\ell x_n}\right\} \tag{23}$$

$$\varphi^w_{ij,2} = c^w_2\frac{\varepsilon}{k}\left(\varphi_{km2}n_k n_m\delta_{ij} - \frac{3}{2}\varphi_{ik2}n_k n_j - \frac{3}{2}\varphi_{jk2}n_k n_i\right)\left\{\frac{k^{1.5}}{\varepsilon c_\ell x_n}\right\}, \tag{24}$$

where

$$\varphi_{ij2} = -c_2\left(P_{ij} = \frac{2}{3}P_k\delta_{ij}\right). \tag{25}$$

Within the viscous sub-layer the wall reflection terms are damped through the function f_w. Their task within the viscous sub-layer is then performed by $(H_{ij} - H_{kk}\,\delta_{ij}/3)$, where H_{ij} is given by equation (26). The contribution of this term is more extensively discussed in Bo *et al.* (1995). It represents a relatively simple way of achieving approximately the correct distribution of the Reynolds

stresses across the viscosity-affected sub-layer, by taking energy from the fluctuating component normal to a wall and redistributing it equally in the other two directions.

$$H_{ij} = f_H \frac{\nu}{k}\left(\rho\,\overline{u_i u_\ell}\frac{\partial\sqrt{k}}{\partial x_\ell}\frac{\partial\sqrt{k}}{\partial x_j} + \rho\,\overline{u_j u_\ell}\frac{\partial\sqrt{k}}{\partial x_\ell}\frac{\partial\sqrt{k}}{\partial x_i}\right). \tag{26}$$

The term J_{ij}, given in equation (27), increases the sensitivity of the model to the effects of low mean flow Reynolds number.

$$J_{ij} = f_J \rho\, k\left(\frac{\partial U_i}{\partial x_j} + \frac{\partial U_j}{\partial x_i}\right). \tag{27}$$

The turbulent heat fluxes are obtained through the generalised gradient diffusion hypothesis, given by equation (28).

$$\overline{u_i t} = -\rho\, c_T \frac{k}{\varepsilon}\overline{u_i u_j}\frac{\partial T}{\partial x_j}. \tag{28}$$

Simplified (zonal) DSM closure. In the *fully turbulent* region, ε is obtained from the same equation used in the high-Re k-ε model. In the *near-wall* region, ε is obtained from the wall distance, as in the Woolfshtein model (1969), but with:

$$\ell_\varepsilon = 2.55\ \mathrm{Y}[1 - \exp(-0.236\ \mathrm{y}*)]. \tag{29}$$

The damping functions that appear in equations (21)-(27) depend on the dimensionless wall distance y* and have the following expressions:

$$\mathrm{f_e} = \exp(-\mathrm{y}^{*}/3) \tag{30}$$

$$\mathrm{f_w} = [1 - \exp(-0.12\mathrm{y}^{*})][1 + \exp(-0.03\mathrm{y}^{*})] \tag{31}$$

$$\mathrm{f_J} = 0.06\exp(-\mathrm{y}^{*}/3) \tag{32}$$

$$\mathrm{f_H} = (10.2 + 7.5\mathrm{y}^{*})\exp(-\mathrm{y}^{*}/20). \tag{33}$$

Low-Re DSM closure. The dissipation rate equation is the same as equation (17) of the Low-Re k-ε model. The damping functions that appear in equations (21)-(27) now depend on the turbulent Reynolds number, R_t, and have the following expressions:

$$\mathrm{f}_\varepsilon = \exp(-\mathrm{R_t}/8) \tag{34}$$

$$\mathrm{f_w} = [1 - \exp(-\mathrm{R_t}/20)][1 - \exp(-\mathrm{R_t}/100)] \tag{35}$$

$$\mathrm{f_J} = 0.06\exp(-\mathrm{R_t}/8) \tag{36}$$

$$f_H = (10 + 2.6R_t)\exp(-R_t/20) \tag{37}$$

Also f_μ, since μ_t still appears in the stress (19) and ε (17) transport equations, is now obtained from:

$$f_\varepsilon = \exp[-4/(1 + 0.01R_t)^2]. \tag{38}$$

As mentioned earlier, the damping functions shown in equations (30)-(38), have been devised with reference to fully-developed pipe flows and not specifically for the ribbed passage flows presented in this study.

Length scale correction terms

It is well known, that in separated flows, the Launder-Sharma version of the ε equation returns excessively high levels of near-wall turbulence. To address this problem, Yap (1987) proposed the addition of a correction term, YC, to the ε equation, equation (17), based on the wall distance, Y:

$$YC = \max\left|0.83\frac{\varepsilon^2}{k}\left(\frac{k^{1.5}/\varepsilon}{2.55Y} - 1\right)\left(\frac{k^{1.5}/\varepsilon^2}{2.55Y}, 0\right)\right. . \tag{39}$$

In a recent proposal by Hanjalic (1996), the wall distance in the above term is eliminated by using the gradient of the length scale normal to the wall surface. Here, these ideas are further developed, by introducing the resultant of the length scale gradient vector, and by also taking into account the effects of wall damping across the sub-layer.

From Woolfshtein:

$$\ell_\varepsilon = 2.55\,Y[1 - \exp(-0.263y^*)]. \tag{40}$$

Differentiating ℓ_ε and then replacing y* by R_t, as proposed by Yap (1987), produces the following expression for the gradient of the equilibrium length scale, $(d\ell_e/dY)$:

$$(d\ell_e/dY) = c_\ell[1 - \exp(-B_\varepsilon R_t)] + B_\varepsilon c_\ell R_t \exp(-B_\varepsilon R_t), \tag{41}$$

with $c_\ell = 2.55$ and $B_\varepsilon = 0.1069$.

From the resultant gradient, $D\ell$, of turbulent length scale $\ell = k^{3/2}/\varepsilon$, a correction factor F is defined according to:

$$D\ell = \{(d\ell/dx_j)(d\ell/dx_j)\}^{1/2} \tag{42}$$

and

$$F = [(D\ell - (d\ell_e/dY)]/c_\ell. \tag{43}$$

A new version of the Yap term can then be developed, NYC of the form:

$$NYC = \max[0.83F(F + 1)^2\rho\varepsilon^2/k, 0]. \tag{44}$$

The modelling constants that appear in the preceding equations have the values given in Table I

4. Numerical aspects

A finite volume solver has been employed, which solves the flow equations in a fixed, Cartesian and axisymmetric co-ordinate system. A semi-staggered grid arrangement is employed, in which the velocity nodes are located at the corners of the scalar control volumes, and, in the second-moment computations, the nodes of all the turbulent stresses are located at the scalar node locations. The cases examined involved passages that are long enough for repeating flow conditions to prevail over each rib interval. Consequently, the numerical flow domain covers only one rib interval, and repeating flow and thermal boundary conditions are applied. A Cartesian mesh is employed, with the grid nodes falling within the ribs blocked off.

Three mesh sizes have been tested, one consisting of 51 × 60 nodes, a finer 91 × 110 mesh and, for the ribbed channel case, an even finer 111 × 130 mesh. In some of the cases examined there were some differences in the Nusselt number levels predicted using the 51 × 60 and the 91 × 110 meshes, but the introduction of the 111 × 130 mesh did not produce any further differences in the predicted Nusselt number. All the results presented here have been obtained using the 91 × 110 mesh, in which 37 grid nodes are used to resolve each side of the rib. In the zonal models, the first 15 grid nodes are within the fixed-length-scale region. The y* value for the near-wall node is of the order of 1, while at the interface between the near-wall and the fully-turbulent regions the y* value is around 100. More details can be found in Raisee (1999).

5. Cases examined

As shown in Figure 1, three types of passage have been examined: an annular passage with a ribbed inner wall, a ribbed pipe, and a plane channel with ribs

Table I. Turbulence modelling constants

c_μ	σ_k	σ_ε	$c_{\varepsilon 1}$	$c_{\varepsilon 2}$	c_1	c_2	$c^w{}_1$	$c^w{}_2$	c_T	σ_T
0.09	1	1.22	1.44	1.92	1.8	0.6	0.5	0.3	0.3	0.9

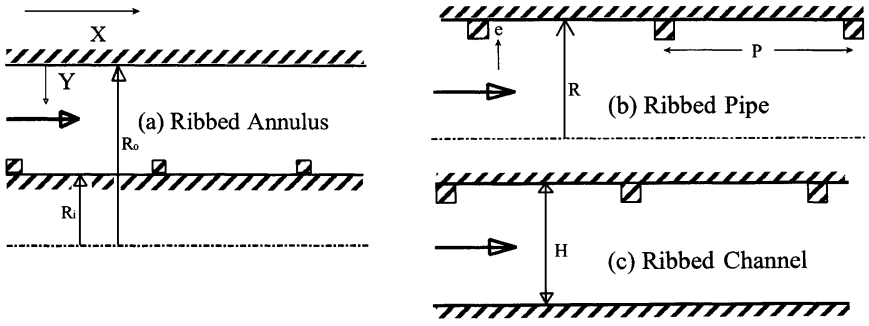

Figure 1. Flow geometries examined

only along one wall. Five cases have been computed in total, with the details presented in Table II. As shown in Figure 1, e denotes the rib height, P the rib spacing, D the pipe diameter and H the channel height. For the annular passage the ratio between the inner and outer radii, $R_I/R_O = 0.392$.

6. Presentation and discussion of results

6.1 Ribbed annular passage

Comparisons between measured and computed mean velocity profiles, for the two annular cases, are presented in Figure 2. The measurements show that the velocity maximum is close to the smooth, outer wall. Near the inner, ribbed wall, there is a sharp drop in velocity, especially when the ribs are closer (P/e = 10.8), implying that closer to the wall, where data are not available, a

Passage geometry	P/e	e/R_o-R_I) or e/D or e/H	Re	Exp. data	Comparisons
Annular passage	20	0.05	30×10^3	Lee *et al.* (1988)	Vel. profile
Annular passage	10.8	0.05	30×10^3	Lee *et al.* (1988)	Vel. profile
Ribbed pipe	10	0.0675	24×10^3	Baughn and Roby (1992)	Local Nu
Ribbed pipe	10	0.0675	64×10^3	Baughn and Roby (1992)	Local Nu
Ribbed channel	10	0.1	122×10^3	Purchase (1991)	Local Nu

Table II. Details of cases computed

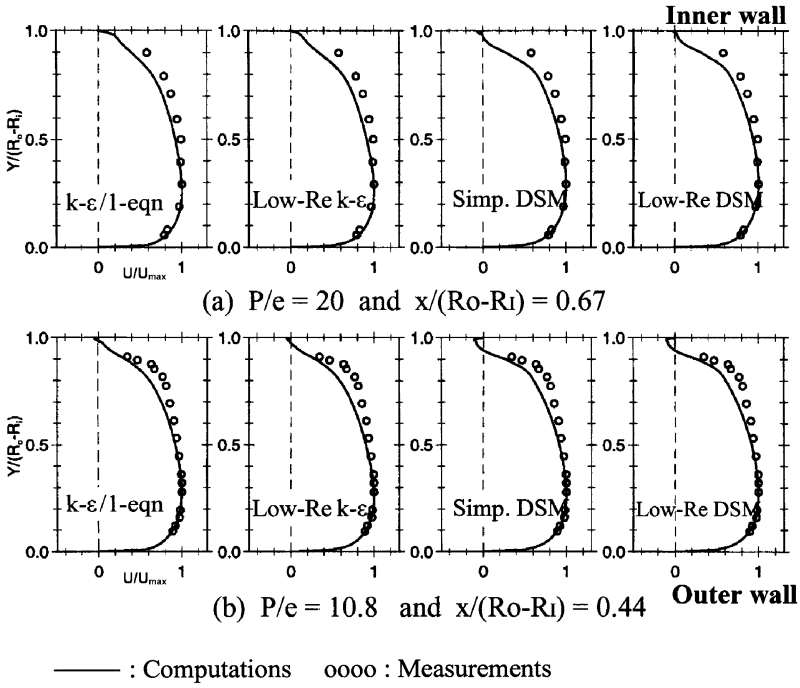

Figure 2. Mean velocity comparisons for annular channel

separation bubble is present. The main features are well reproduced by the computations, but a more gradual reduction in velocity is returned at the ribbed wall, especially by the effective viscosity models. The DSM profiles, for P/e = 10.8, show a larger separation bubble than their EVM counterparts, which is more consistent with the data. The different approaches to near-wall modelling do not appear to influence the mean flow predictions.

6.2 Ribbed pipe

For the ribbed pipe flows, local Nusselt number comparisons are shown in Figures 3 and 4, for Reynolds numbers of 24×10^3 and 64×10^3 respectively. Both zonal models (k-ε/1-eqn and simplified DSM), though not in complete accord with the measurements, nevertheless produce reasonable Nu levels at the two Reynolds numbers (Figures 3(a) and 4(a)). Immediately downstream of the rib, where the flow has separated, the zonal EVM predicts that the peak Nusselt number occurs too close to the rib, in comparison with the data, while the zonal DSM, again in comparison to the data, predicts the rise to be too slow. These predictive differences are consistent with the fact that, as shown in Figure 2, the DSM models return a larger separation bubble. Both models under-predict the maximum Nu level associated with flow re-attachment. This is not unexpected, since in separated flows the assumption that the turbulent length scale is proportional to the wall distance breaks down. After re-attachment, the thermal predictions of both zonal models and especially the DSM are in good agreement with the data. Over the rib itself, the Nusselt number levels are well predicted by the k-ε/1-eqn model, while with the simplified DSM they are under-predicted, especially at the higher Reynolds number. On the whole, the two simpler, zonal models produce thermal

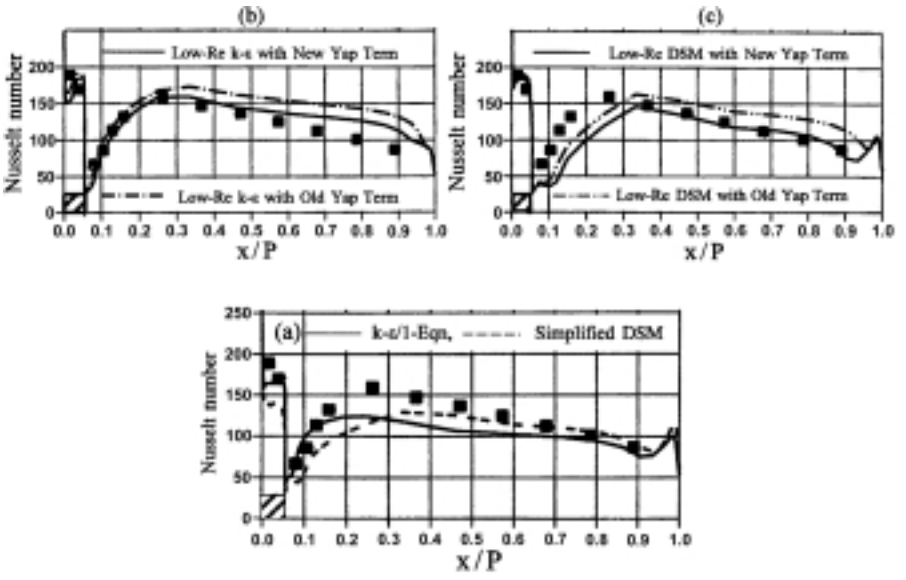

Figure 3.
Local Nusselt number comparisons for flow through the ribbed pipe at Re = 24×10^3

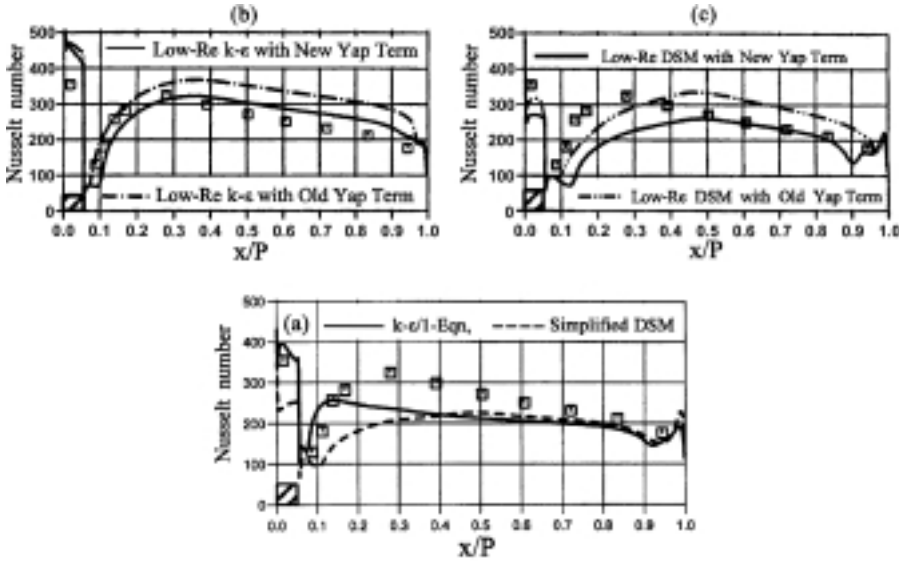

Figure 4.
Local Nusselt number comparisons for flow through the ribbed pipe at Re = 64×10^3

predictions that in the ribbed pipe investigated are surprisingly close to the experimental data. The fact that at the higher Reynolds number the differences between the predicted and measured levels is greater suggests that the Reynolds number effect on the Nusselt number is not fully reproduced by the zonal approach to the modelling of near-wall turbulence.

The low-Re k-ε predictions, shown in Figures 3(b) and 4(b), reveal that abandoning the near-wall length scale approximation considerably improves the predicted thermal behaviour in the separation region, returning the correct recovery from the rib corner. While with the old Yap term the Nu levels are noticeably over-predicted, introduction of the new Yap term leads to more satisfactory Nusselt number computations along the pipe wall. At the higher Reynolds number, Nu levels over the rib are however over-predicted. Computations without any Yap term have not been included because they produced Nu levels substantially higher than those measured.

For the low-Re DSM, Figures 3(c) and 4(c) show that, as also noted in the zonal DSM comparisons, a more gradual rise in Nu levels downstream of the rib is produced, which for the ribbed-pipe-flows is in contrast to the measured behaviour. With the old Yap term, Nusselt number levels over the downstream half of the rib interval, after re-attachment, are over predicted. The new Yap term again lowers the predicted Nu levels, leading to very close agreement with the experimental data over the downstream half of the rib interval. Nusselt number levels are, however, severely under predicted, over the upstream half of the rib interval, within the separation region. The low-Re DSM computations are somewhat closer to the data than the corresponding zonal computations, but not as close as the low-Re EVM predictions. For both low-Re models, but especially the EVM, introduction of the new Yap term, which is independent of

the wall distance, leads to improvements in the heat transfer predictions. Our examination of the predicted flow fields at Re = 24,000 was not sufficiently detailed to allow us to identify why the low-Re DSM predictions display the rather unrealistic sharp changes in the profiles of the local Nusselt number at x/P of 0.33, where the local Nu reaches its maximum level.

6.3 Ribbed channel

For the plane ribbed channel, the computed flow field and near-wall distribution of the turbulence energy are presented in Figures 5 and 6, respectively. The separation bubble downstream of each rib now extends over almost half the rib interval. A smaller separation bubble is formed ahead of each rib. The predicted k levels are considerably higher than those found in smooth passages, but are consistent with those observed in recent experimental studies (Iacovides *et al.*, 1996). Within the separation bubble, the new Yap term

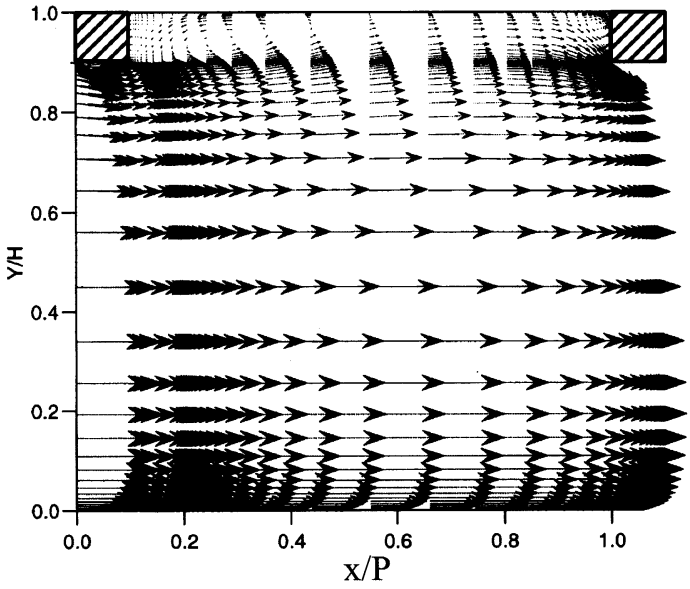

Figure 5.
Predicted mean flow in the ribbed channel

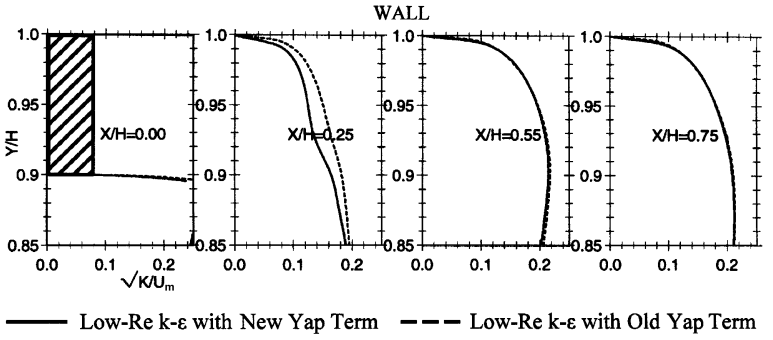

Figure 6.
Near-wall profiles of turbulent kinetic energy, for flow through the ribbed channel

returns somewhat lower turbulence levels than the old version; a feature consistent with the heat transfer comparisons.

Local Nusselt number comparisons for the plane ribbed channel are shown in Figure 7. The measurements indicate that the Nusselt number now rises more gradually downstream of the rib, reaching the maximum level at around the half-way point of the interval. This behaviour is markedly different from that observed in the ribbed pipe. One possible explanation for this difference in the Nusselt number distribution is that the rib-size for this case is larger than for the ribbed pipe. Data for three-dimensional flows through ribbed ducts (Baughn and Yan, 1992), however, suggest that another probable cause for this difference in behaviour is the fact that now a plane ribbed surface is examined, while in the previous case the ribbed surface was axi-symmetric.

The k-ε/1-eqn model of Figure 7(a) produces a more gradual rise in Nu than for the ribbed pipe at Re = 64 $\times$ 10^3 of Figure 4(a), but still, in comparison with the experimental data, predicts the location of peak Nu too close to the rib. As also observed earlier, over most of the rib interval, heat transfer levels are under-predicted by the zonal EVM model. Along the top surface of the rib, this model returns the correct variation of the Nusselt number, but over-predicts the level. The zonal DSM, on the other hand, while still under-estimating heat transfer levels, nevertheless produces the correct variation over the rib interval. Along the top surface of the rib, the peak Nu level is predicted to occur too close to the downstream corner of the rib, but the levels are closer to those measured. On the whole, the predictions of the zonal DSM are closer to the measurements than those of the zonal EVM.

As also noted in the ribbed pipe comparisons, replacing the zonal EVM by the low-Re k-ε, Figure 7(b), results in a more gradual increase in the Nusselt

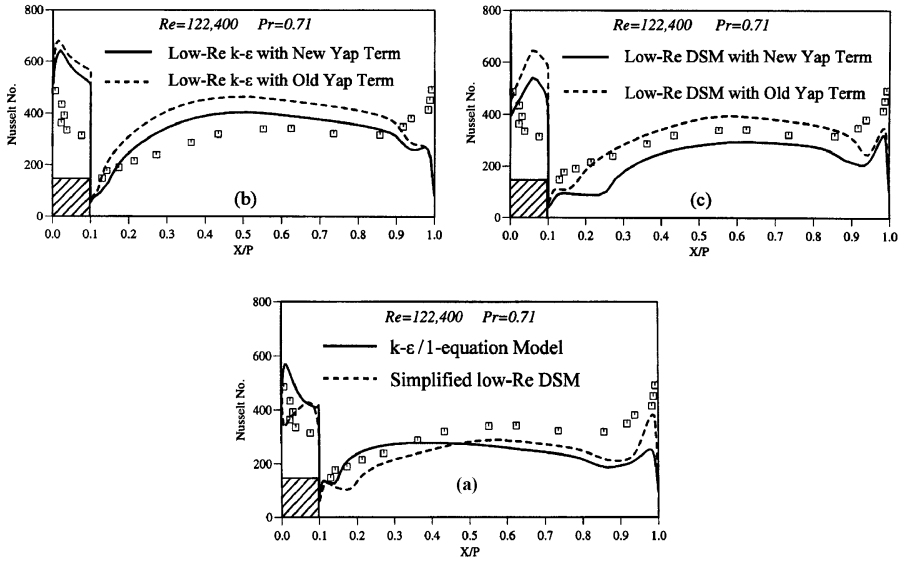

Figure 7.
Local Nusselt number comparisons for flow through the ribbed plane channel

number downstream of the rib and also in higher Nu levels. The predicted Nu levels are now higher than the measured values and the peak Nu in the rib interval is still predicted to be closer to the upstream rib than the measured peak. The new Yap term leads to lower Nu levels, thus improving thermal predictions. The computed levels, however, still remain higher than those measured, especially over the rib.

The low-Re DSM, Figure 7(c), like its zonal counterpart, returns a gradual rise in Nusselt number downstream of the rib, which is consistent with the experimental behaviour. With the old Yap term, the DSM model overestimates somewhat heat transfer levels over part of the rib interval and even more so over the rib surface. With the new Yap term, wall heat transfer over the rib interval is somewhat under-predicted, while over the rib surface its computed level is closer to the measurements than that of the Low-Re EVM. In common with the zonal DSM, however, over the rib surface the two low-Re DSM closures predict that the peak Nu level occurs over the downstream half of the rib. This is in contrast to the measured variation and also to that predicted by the effective-viscosity models. Close-up plots of the predicted flow field over the rib, shown in Figure 8, reveal that the EVM closures predict that only a small separation bubble is formed at the upstream corner of each rib, followed by re-attachment, while the DSM closures return a longer separation bubble, with re-attachment over the downstream half of the rib surface. This explains the differences in the predicted variations in local Nusselt number over the rib surface. On the whole, the new Yap term improves the DSM predictions. The most serious discrepancy occurs in the upstream corner, where heat transfer levels are seriously underestimated. This feature is also present, though not as strong, in the DSM computations for the ribbed pipe. It thus appears that the DSM models employed here over-damp turbulence in corner regions. A probable cause of this over-damping of turbulence could be the use of the wall reflection terms, φ_{ij}^{W}, and the other damping term H_{ij}, both of which have been developed with reference to the damping effects of a single wall. In corner regions, these terms may thus lead to excessive damping of turbulence. The fact that this feature is stronger in the ribbed channel case may be due to the fact that in this case the rib size is greater.

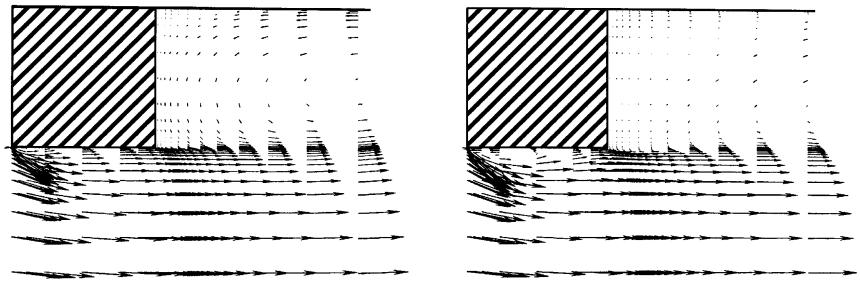

Figure 8.
Predicted flow fields over rib, for flow through ribbed channel

In general, heat transfer predictions for the ribbed channel are not as close to the data as the corresponding predictions for the ribbed pipe, especially over the rib surface. In addition to the difference in the passage geometry, the rib is larger and the flow Reynolds number is considerably higher than those in the ribbed pipe computations. The grid refinement tests have shown that numerical errors cannot account for the observed predictive deficiencies. One possible explanation is that the turbulence models employed find it more difficult to cope with the effects of the larger separation bubble, caused by the larger rib. A second explanation, for which the two sets of computations for the ribbed pipe provide some support, is that the models employed do not fully reproduce the Reynolds number effect on heat transfer. The ribbed pipe comparisons of Figures 3 and 4 show that differences between the Nusselt number computations produced by the zonal and the low-Re DSM models and the experimental data are greater at the higher of the two Reynolds numbers examined. Moreover, this Reynolds-number-related trend in predictive deficiencies observed in the ribbed pipe comparisons is consistent with the somewhat greater predictive deficiencies identified in the comparisons between the computed Nusselt number distributions of the zonal and low-Re DSM models and the experimental data for the ribbed channel. Finally, a parallel study within the author's group (Craft *et al.*, 1999), looking at heat transfer predictions in an abrupt pipe expansion, has also reached a similar conclusion regarding the ability of turbulence models to reproduce the Reynolds number effect on Nusselt number in recirculating flows.

7. Concluding remarks

From the comparisons presented, a number of conclusions may be drawn on the use of low-Re models flow and heat transfer computations in two-dimensional ribbed passages.

Zonal models that obtain the near-wall dissipation rate from the wall distance have performed better than expected, returning reasonable, though lower than the measured, overall heat transfer levels. Their main weakness is in the prediction of wall heat transfer in the separation bubble, downstream of the rib. Nevertheless, in plane ribbed channels, the thermal development over the entire passage is closely mimicked by the zonal DSM.

The *low-Re* computations reveal that even with the Yap term, both models tested, and the EVM in particular, overestimate Nusselt number levels. An alternative correction term is proposed, which is independent of the wall distance, though based on the same empirical arguments as the Yap term. This new term improves the thermal predictions of both low-Re models tested. Neither of the two low-Re models, however, returns thermal predictions that are in complete agreement with the measurements. In ribbed pipes the thermal behaviour is well reproduced by the low-Re EVM. The low-Re DSM produces the correct behaviour after re-attachment, but not a fast enough recovery downstream of the rib. For ribbed plane channels, the variation in local Nusselt number is more faithfully reproduced by the low-Re DSM model, though the

level is under-predicted. The low-Re EVM returns a faster Nusselt number recovery downstream of the rib and substantially over-predicts its level over the rib.

The comparisons show that while for the passage geometry closer to that of a blade cooling passage, namely the plane ribbed channel, the DSM models (zonal and low-Re) produce realistic simulations of the thermal behaviour, the rather simple DSM versions tested here do not always return the correct thermal behaviour in the rib-induced separation regions. Thus, even though the heat transfer predictions are for the most part acceptable, more effective closures need to be developed.

Another deficiency of the turbulence models tested appears to be their inability to fully reproduce the Reynolds number effect on the Nusselt number in ribbed passages. This suggests that numerical studies aiming to assess and develop turbulence models suitable for heat transfer predictions through ribbed passages should carry out comparisons over a wide range of Reynolds numbers.

References

Baughn, J.W. and Roby, J. (1992), *ASME 28th National Heat Transfer Conference*, HTD-Vol. 202, San Diego, CA.

Baughn, J.W. and Yan, X. (1992), "Local heat transfer measurements in square ducts with transverse ribs", ASME, National Heat Transfer Conference.

Besserman, D.L. and Tanrikut, S. (1991), "Comparison of heat transfer measurements with computations for turbulent flow around a 180° bend", ASME Paper 91-GT-2, International Gas-Turbine and Aero Congress, Orlando, FL.

Bo, T., Iacovides, H. and Launder, B.E. (1995), "Developing buoyancy-modified turbulent flow in ducts rotating in orthogonal mode", *ASME Journal of Turbomachinery*, Vol. 117, pp. 474-84.

Craft, T.J., Iacovides, H. and Yoon, J.H. (1999), "Progress in the use of non-linear two-equation models in the computation of convective heat-transfer in impinging and separated flows", *Flow, Turbulence and Combustion*, Vol. 63, pp. 59-80.

Gibson, M.M. and Launder, B.E. (1978), "Ground effects on pressure fluctuations in atmospheric boundary layers", *Journal of Fluid Mechanics*, Vol. 85, p. 391.

Hanjalic, K. (1996), "Some resolved and unresolved issues in modelling non-equilibrium and unsteady turbulent flows", Proceedings of the 3rd International Symposium on Engineering Turbulence Modelling and Measurements, Crete.

Iacovides, H. and Launder, B.E. (1992), "The computation of convective heat transfer in a 180° pipe bend", ICHMT, International Symposium Heat Trans. in Turbomachinery, Athens.

Iacovides, H. and Launder, B.E. (1995), "Computational fluid dynamics applied to internal cooling of gas-turbine blade cooling: a review", *International Journal Heat and Fluid Flow*, Vol. 16, pp. 454-70.

Iacovides, H. and Toumpanakis, P. (1993), "Turbulence modelling of flow in axisymmetric rotor-stator systems", Proceedings of IAHR, 5th International Symposium on Refined Flow Modelling and Turbulence Measurements, Paris.

Iacovides, H., Jackson, D.C., Ji, H., Kelemenis, G., Launder, B.E. and Nikas, K. (1996), "LDA study of flow development through an orthogonally rotating U-bend of strong curvature and rib-

roughened walls", Paper No. ASME-96-GT-476, International Gas-Turb and Aero Congress, Birmingham.

Launder, B.E. and Sharma, B.I. (1974), "Application of the energy-dissipation model of turbulence to the calculation of flow near a spinning disc", *Letrs in Ht Mass Trans.*, Vol. 1, pp. 131-8.

Lee, B.K., Cho, N.H. and Choi, Y.-D. (1988), "Analysis of periodically fully developed turbulent flow and heat transfer by k-ε equation model in artificially roughened annulus", *International Journal of Heat Mass Transfer*, Vol. 31, pp. 1797-806.

Liou, T.-M., Hwang, J.-J. and Chen, S.-H. (1993), "Simulation and measurement of enhanced turbulent heat transfer in a channel with periodic ribs on one principal wall", *International Journal of Heat and Mass Transfer*, Vol. 36, pp. 507-17.

Nikas, K.S. (2000), "The computation of flow and heat transfer through stationary and orthogonally rotating U-bends", PhD thesis, Department of Mechanical Engineering, UMIST, Manchester.

Purchase, G. (1991), private communication.

Raisee, M. (1999), "Computation of flow and heat transfer through two- and three-dimensional rib-roughened passages", PhD thesis, Department of Mechanical Engineering, UMIST, Manchester.

Taylor, C., Xia, J.Y., Medwell, J.O. and Morris, W.D. (1991), "Numerical simulation of three-dimensional turbulent flow and heat transfer within a multi-ribbed cylindrical duct", ASME Paper 91-GT-8, International Gas-Turbine and Aero Congress, Orlando, FL.

Woolfshtein, M. (1969), "The velocity and temperature distribution in one-dimensional flow with turbulence augmentation and pressure gradient", *International Journal of Heat and Mass Transfer*, Vol. 12, p. 301.

Yap, C.R. (1987), "Turbulent heat and momentum transfer in recirculating and impinging flows", PhD thesis, Department of Mechancial Engineering, Faculty of Technology, UMIST Manchester.